Comparison of Injection-Locked and Coupled Oscillator Arrays for Beamforming

Yu-Tsung Lo and Jean-Fu Kiang

***Abstract*—Injection-locked oscillator arrays (ILOAs) and coupled oscillator arrays (COAs) are analyzed using Adler's equation, and their performance to drive phased arrays for beam-steering is compared. The Monte Carlo simulation results indicate that COAs render smaller beam-pointing error when the locking range of oscillators is narrow (high Q), while ILOAs render smaller beam-pointing error when the locking range is wide (low Q). An ILOA with a frequency tripler connected to the oscillators' output is designed to increase the achievable range of inter-element phase shift, and a chip is fabricated in the TSMC 0.18-μm CMOS technology to verify the design concept, with the measured maximum phase shift around 240°.**

***Index Terms*—Adler's equation, beam-steering, coupled oscillator array (COA), frequency tripler, injection-locked oscillator array (ILOA), Monte Carlo simulation, mutual locking, quality factor, voltage-controlled oscillator (VCO).**

I. Introduction

THE OUTPUT power of oscillators can be combined via a power-combining network before feeding the antenna elements [1]. Spatial power combining is an alternative way to combine the output power of all the oscillators with proper synchronization [2], which can be implemented using injection-locked oscillator arrays (ILOAs) or coupled oscillator arrays (COAs) [3]. A linear phase progression over the oscillators can be obtained by tuning the free-running frequencies of these oscillators [4]. Such oscillator arrays can be used to conduct beamforming by serving as the local oscillators (LOs) [5] or by directly feeding the antenna elements [6], [7].

In a typical ILOA, each oscillator is independently controlled by adjusting its free-running frequency. All the oscillators in an ILOA are locked via an external injection signal to oscillate at the desired frequency. The output phase of each oscillator, relative to the injection phase, is determined by the difference of its free-running frequency and the frequency of the injection signal.

In a typical COA, all the oscillators are connected via a coupling network. The phase progression over the oscillators is achieved by tuning the free-running frequencies of the oscillators at both ends [8], or changing the phase difference between these two oscillators via phase shifters [9].

The behaviors of ILOAs and COAs can be predicted from the governing equation of nonlinear oscillators [3]. The Adler's equation [10] has been used to relate the output phase of an oscillator to the phase of the injection signal, which can also be used to model the behavior of ILOAs. Since the maximum achievable phase difference of the two end oscillators in an ILOA is $\pm 90^\circ$, the progressive phase difference of an N-element ILOA is restricted to $180^\circ/(N-1)$. Adler's equation has been applied to analyze COAs as well. Both ILOAs and COAs have been implemented, including a 4-GHz ILOA with GaAS MESFET oscillators [11], an ILOA implemented as a quasi-real-time spectrum analyzer [12], a three-element COA with optimal coupling phase [13], and a four-element COA with a maximum beam-steering angle of 10° at 10 GHz [14].

The free-running frequency of a voltage-controlled oscillator (VCO) may deviate due to variations of process, supply voltage, and temperature. Such frequency deviations will affect the performance of ILOAs and COAs, which will in turn affect the beam-pointing accuracy of the phased arrays they drive. In this work, a Monte Carlo technique is applied to estimate the beam-pointing errors due to deviation of the VCOs' free-running frequency. The beam-pointing errors of ILOAs and COAs are compared under high Q and low Q condition, respectively. In addition, an ILOA chip is implemented to verify the predicted results.

In Section II, the Adler's equation and its extension to govern ILOAs and COAs are briefly reviewed; a fourth-order Runge–Kutta method is used to solve these equations for the time evolution of instantaneous frequency and phase. In Section III, a Monte Carlo technique is applied to simulate these arrays under low Q and high Q condition, respectively. In Section IV, a chip implementation of the ILOA is presented and the measured results are compared with the prediction. Finally, a conclusion is drawn in Section V.

II. Transient Behavior of ILOAs and COAs

Fig. 1(a) shows the configuration of an ILOA. The free-running frequency of each VCO is adjusted by tuning its control voltage. By injecting a common signal, VCOs falling within the locking range will be locked. The relative phase shift of each oscillator can be controlled by tuning its free-running frequency. Note that the difference between the injection phase and the resulting phase of an oscillator can also be obtained with proper design of VCOs and the coupling network among them [15], which is equivalent to tuning the oscillator's Q factor and the injection strength. In this work, we will focus on tuning the frequency.

Manuscript received June 20, 2014; revised January 26, 2015; accepted January 31, 2015. Date of publication February 25, 2015; date of current version April 02, 2015. This work was supported by the National Science Council, Taiwan 106 under Contract NSC 102-2221-E-002-043.

Y.-T Lo was with the Department of Electrical Engineering and the Graduate Institute of Communication Engineering, National Taiwan University, Taipei 106, Taiwan. He is now with VIA Telecom (VTC), Taipei 231, Taiwan.

J.-F. Kiang is with the Department of Electrical Engineering and the Graduate Institute of Communication Engineering, National Taiwan University, Taipei 106, Taiwan (e-mail: jfkiang@ntu.edu.tw).

Color versions of one or more of the figures in this paper are available online at http://ieeexplore.ieee.org.

Digital Object Identifier 10.1109/TMTT.2015.2403847

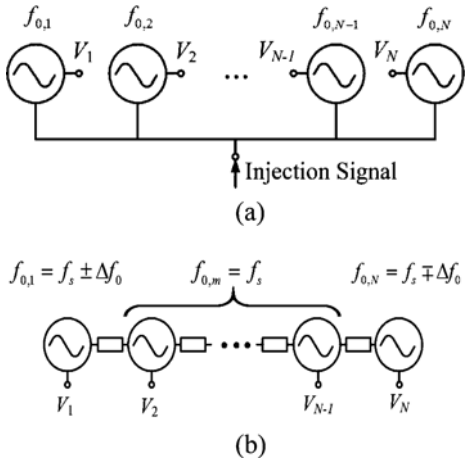

Fig. 1. Configuration of: (a) ILOA and (b) COA.

Fig. 1(b) shows the configuration of a COA without any external injection signals. For a 1-D array, each oscillator is coupled to its adjacent one or two neighbors, and the coupling to farther oscillators is neglected. A linear phase progression over the array can be achieved by tuning the free-running frequencies of the two end elements.

The free-running frequency of each oscillator in an ILOA needs to be tuned. As for a COA, only the two outmost oscillators need to be tuned, and the free-running frequencies of the other $N-2$ oscillators are maintained the same as the target frequency.

A. ILOAs

The behavior of an ILOA, within the locking range of the oscillators, can be modeled using Adler's equation as [3], [10]

$$\frac{d\phi_m}{dt} = \omega_{0,m} - \omega_{\text{inj}} - \frac{\omega_{0,m}}{2Q}\frac{I_{\text{inj}}}{I_m}\sin(\phi_m - \phi_{\text{inj}}) \qquad (1)$$

where ω_{inj} and ϕ_{inj} are the injection frequency and injection phase, respectively; $\omega_{0,m}$ and ϕ_m are the free-running frequency and output phase, respectively, of the mth oscillator; I_{inj} and I_m are the injection amplitude and the free-running amplitude, respectively. The derivation of Adler's equation based on the phasor diagram can be found in [16]. In [8], two differential equations governing the amplitude and phase are derived from the physical model of oscillators, and the Adler's equation is the special case when the amplitude variation is neglected.

The instantaneous output frequency, ω_m, of the mth oscillator can be represented as

$$\omega_m = \omega_{\text{inj}} + \frac{d\phi_m}{dt} = \omega_{0,m} - \frac{\omega_{0,m}}{2Q}\frac{I_{\text{inj}}}{I_m}\sin(\phi_m - \phi_{\text{inj}}). \qquad (2)$$

When ω_m is locked to the injection frequency, ω_{inj}, (1) implies $d\phi_m/dt = 0$. The output phase of the mth oscillator relative to the injection phase can be controlled by the difference between ω_{inj} and $\omega_{0,m}$. At the steady state, the phase difference becomes

$$\phi_m - \phi_{\text{inj}} = \sin^{-1}\frac{\omega_{0,m} - \omega_{\text{inj}}}{\Delta\omega_L} \qquad (3)$$

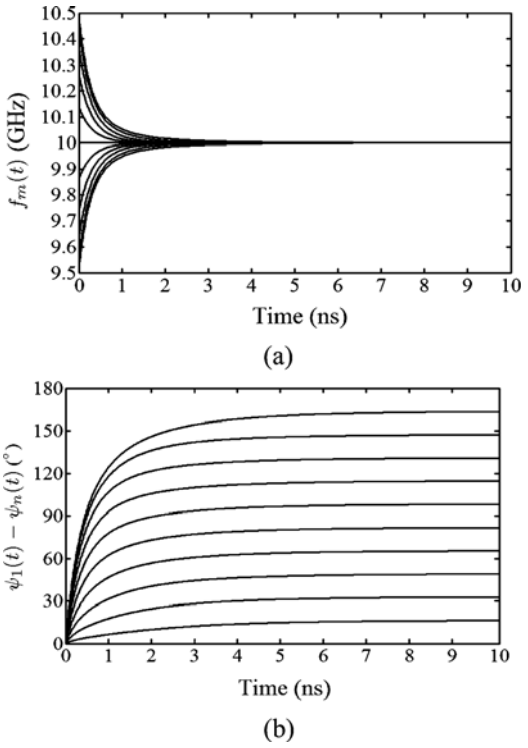

Fig. 2. Time evolution of: (a) instantaneous frequency and (b) phase difference with respect to the first oscillator of an 11-element ILOA.

where

$$\Delta\omega_L = \frac{\omega_{0,m}}{2Q}\frac{I_{\text{inj}}}{I_m} \qquad (4)$$

is the locking range, which is the maximum allowable frequency difference between ω_m and ω_{inj}.

Equation (3) implies that the phase shift after injection locking is restricted to the range $-90^\circ < \phi_m - \phi_{\text{inj}} < 90^\circ$. For an N-element ILOA with linear phase progression, the free-running frequency of each oscillator is tuned to achieve a constant inter-element phase difference, $\alpha_z = \phi_m - \phi_{m+1}$, with $m = 1, 2, \ldots, N-1$. Hence, the maximum allowable inter-element phase difference becomes $180^\circ/(N-1)$.

Fig. 2 shows the transient response of an 11-element ILOA by solving (1) with the fourth-order Runge-Kutta method [17]. The quality factor of oscillators is $Q = 10$, and the injection frequency is 10 GHz. Each curve in Fig. 2(a) shows the time evolution of instantaneous frequencies of all the oscillators. Each curve in Fig. 2(b) shows the phase differences of all the oscillators with respect to the first one. The oscillator with free-running frequency falling within the locking range will be locked to the injection frequency of 10 GHz.

The injection frequency is set to 10 GHz. The two outmost oscillators are tuned apart from 10 GHz by $\pm 0.99\Delta\omega_L$, respectively, leading to a phase difference of 164° between these two oscillators. The maximum inter-element phase difference of this 11-element ILOA is 16.4°. By substituting an integer multiple of this phase difference into (3) one step at a time, the free-running frequencies of the other $N-2$ oscillators can be obtained.

The maximum inter-element phase difference is about 16.4° by simulation when 99% of the locking range is used, compared with the theoretical value of 18° when the full locking range is

used. Here we choose $0.99\Delta\omega_L$ instead of $\Delta\omega_L$ in the simulation because the initial condition of $\omega_{0,m} = \omega_{\text{inj}} \pm \Delta\omega_L$ leads to a numerically unstable solution.

B. COAs

Consider a linear COA of N elements, the instantaneous frequency of the mth oscillator is affected by the other $N-1$ oscillators, and can be modeled by a generalized Adler's equation as [8], [18]

$$\frac{d\psi_m}{dt} = \omega_{0,m} - \frac{\omega_{0,m}}{2Q}\sum_{n=1}^{N}\varepsilon_{mn}\frac{I_n}{I_m}\sin(\xi_{mn} + \psi_m - \psi_n) \quad (5)$$

where ψ_m and $\omega_{0,m}$ are the instantaneous phase and the free-running frequency, respectively, of the mth oscillator; ε_{mn} and ξ_{mn} are the amplitude and phase, respectively, of the complex coupling coefficient between oscillators n and m. If all the oscillators are uncoupled, (5) is reduced to a set of independent oscillators, with the free-running frequency of the mth oscillator being $\omega_{0,m}$.

Note that ψ_m in (5) is the instantaneous phase of oscillator m, while ϕ_m in (1) refers to the phase of oscillator m with respect to the injected signal. Hence, the instantaneous frequency is $d\psi_m/dt = \omega_m$ in (5), and is $\omega_{\text{inj}} + d\phi_m/dt$ in (1). In the steady state, all the oscillators of a COA within the locking range are locked to a common frequency ω_s. In comparison, all the oscillators within the locking range of an ILOA are locked to the injection frequency.

Consider the special case of $N = 2$, with $\varepsilon_{12} = 1$, $\xi_{12} = 0$ and $\varepsilon_{11} = 0$. By substituting $d\psi_m/dt = d\phi_m/dt + \omega_{\text{inj}}$ into (5), the Adler's equation in (1) is obtained.

Take another example, by setting $\xi_{mn} = 2\pi$ in (5), a constant phase progression can be acquired by tuning the free-running frequencies of the two end oscillators, one up and the other down, and tuning those of the other oscillators to $\omega_{0,m} = \omega_s$ with $2 \le m \le N-1$ [8].

Equation (5) has been studied using a perturbation analysis [8], which concludes that the inter-element phase difference is restricted to the range $-90^\circ < \Delta\psi < 90^\circ$ when $\xi_{mn} = 0^\circ$. If the COA is used to feed a linear N-element antenna array at a uniform spacing of half wavelength, the major lobe of the radiation pattern will cover $\pm 30^\circ$ about the broadside direction.

Fig. 3 shows the transient response of an 11-element COA, by solving (5) with the fourth-order Runge-Kutta method. The coupling phase between two nearby oscillators is $\xi_{mn} = 2\pi$. The two outmost oscillators are tuned apart from 10 GHz by $\pm 0.99\Delta\omega_L$, respectively, and the other oscillators are tuned to 10 GHz. Each curve in Fig. 3(a) represents the instantaneous frequency of an oscillator. Each curve in Fig. 3(b) represents the phase difference between the mth oscillator and the first one. The oscillators with free-running frequency falling within the locking range are locked to a common frequency of 10 GHz. The maximum inter-element phase difference is about 81.8°, which is much larger than that of an ILOA.

Take a closer look at Figs. 2(a) and 3(a) in the early stage of the locking process. For the COA, the instantaneous frequencies, ω_m with $2 \le m \le N-1$ are first pulled apart and then locked (synchronized) toward the desired frequency, ω_s. As for the ILOA, all the instantaneous frequencies drift toward the injection frequency from the beginning.

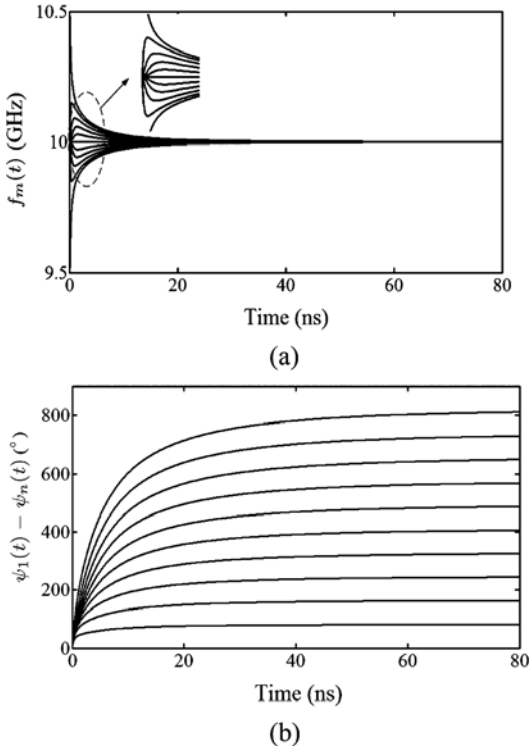

Fig. 3. Time evolution of: (a) instantaneous frequency and (b) phase difference with respect to the first oscillator of an 11-element COA.

III. Simulations on Beam-Pointing Error

The free-running frequency of each oscillator usually deviates from its designed value, which can be characterized by a standard deviation σ_f. Such frequency deviation is different from the short-term phase noise attributed to thermal noise or flicker noise, and will cause little problem to typical communication systems as long as its rate of change falls within the bandwidth of the phase-locked loop (PLL) [19]. However, such frequency deviation will cause a beam-pointing error of a linear antenna array driven by the oscillator array. A specific circuit [20] has been designed to compensation for the frequency deviation.

In this section, the Monte Carlo technique is applied to simulate the beam-pointing error of a linear antenna array driven by the oscillator arrays operating at 10 GHz. A total of 5000 realizations are generated. In each realization, the free-running frequency of each VCO is assigned on a Gaussian distribution, which is then substituted into (1) and (5) to analyze the transient behavior of an ILOA and a COA, respectively.

In practice, the oscillator amplitude varies with the free-running frequency within the tuning range. Hence, the Monte Carlo simulation is restricted to the in-phase condition, with the free-running frequency of all the oscillators set equal.

The fourth-order Runge-Kutta method [17] is used to solve these nonlinear differential equations. If any of the oscillators in an array fails to lock into the target frequency of 10 GHz, within 1-MHz frequency deviation, the associated realization is claimed as an unlock case. The probability of lock, P_{lock}, is

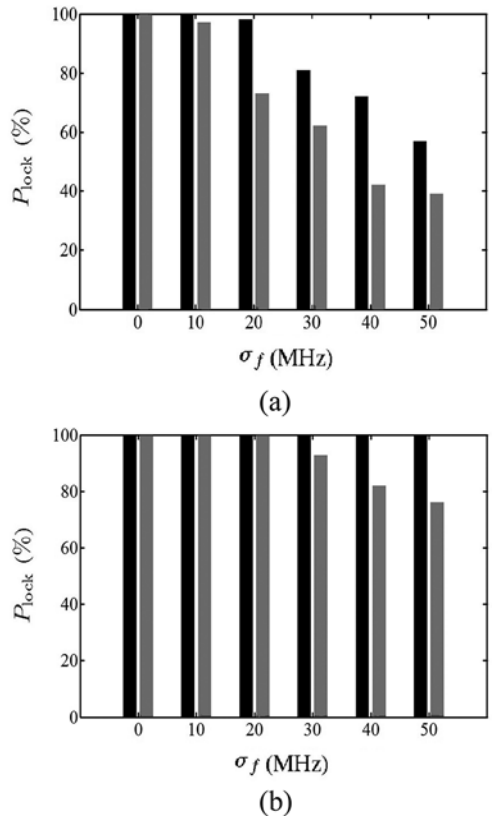

Fig. 4. Probability of lock of 11-element ILOA (dark bar) and COA (grey bar), under in-phase condition: (a) $Q = 62.836$ and (b) $Q = 10$.

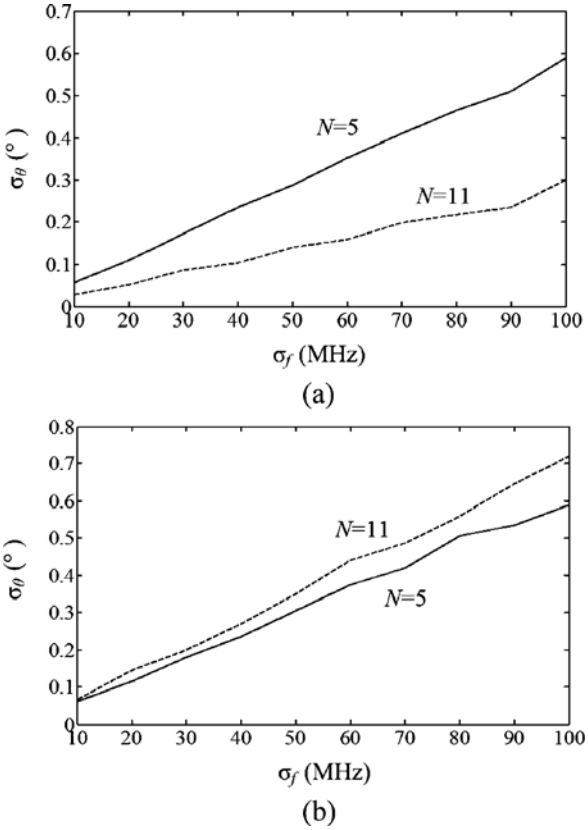

Fig. 5. Simulated standard deviation of beam-pointing error, σ_θ, of: (a) ILOA and (b) COA with respect to σ_f. $Q = 10$, —: $N = 5$, – – –: $N = 11$.

TABLE I
SIMULATED BEAM-POINTING ERRORS WITH $Q = 62.836$

σ_f(MHz)	N	COA [26]		COA (this work)		ILOA (this work)	
		$\langle\theta\rangle$(°)	σ_θ(°)	$\langle\theta\rangle$(°)	σ_θ(°)	$\langle\theta\rangle$(°)	σ_θ(°)
100	5	−0.006	3.08	0.11	3.86	0.29	14.99
80	7	−0.051	2.84	0.09	3.3	−1.03	13.04
50	11	0.017	2.17	0.05	2.3	−0.38	7.85
50	15	0.017	2.46	−0.06	2.33	−0.12	9.44

TABLE II
SIMULATED BEAM-POINTING ERRORS WITH $Q = 10$

σ_f(MHz)	N	COA (this work)		ILOA (this work)	
		$\langle\theta\rangle$(°)	σ_θ(°)	$\langle\theta\rangle$(°)	σ_θ(°)
100	5	−0.017	0.59	0.009	0.59
80	7	0.016	0.49	0.030	0.35
50	11	−0.012	0.35	0.005	0.14
50	15	−0.012	0.37	0.002	0.11

defined as the ratio between the number of locked cases and the total number of realizations.

Fig. 4 shows the probability of lock of an ILOA and a COA, respectively, each having 11 elements. The probability of lock decreases as σ_f is increased, under a given α_z; and it also decreases as α_z is increased. As was discussed in Section II-A, the maximum allowable inter-element phase difference is $\alpha_z = 180^\circ/(N-1)$, which is achieved by pushing the two end oscillators to the limit of their locking bandwidth. For the ILOA, the largest α_z is obtained when the free-running frequencies of the two end oscillators are tuned to $0.99\Delta\omega_L$ and $-0.99\Delta\omega_L$, respectively, off the target frequency; while those of the other oscillators are interpolated between these two frequencies. For the COA, the largest α_z is obtained when the free-running frequencies of the two end oscillators are tuned to $0.99\Delta\omega_C$ and $-0.99\Delta\omega_C$, respectively, off the target frequency; while those of the other oscillators are set to 10 GHz. The P_{lock} of the ILOA is higher than that of the COA since the former benefits from an external injection signal.

Consider an N-element linear antenna array arranged along the x-axis with a uniform spacing of $d = \lambda/2$. The array factor of the radiation pattern can be derived as [21]

$$F(\theta) = \sum_{p=1}^{N} e^{j(p-1)(kd\sin\theta - \alpha_z)} \tag{6}$$

where k and θ are the wavenumber and the zenith angle, respectively, α_z is the inter-element phase difference of the array, which is the same as that of the driving oscillator array. After all the oscillators are locked (in ILOA) or synchronized (in COA) to 10 GHz within 200-kHz bandwidth, the phases of the oscillators are taken to calculate the array factor.

In the simulation, the main beam is steered to the broadside, with $\alpha_z = 0$. Again, the Monte Carlo technique is applied to estimate the beam-pointing error and its standard deviation of

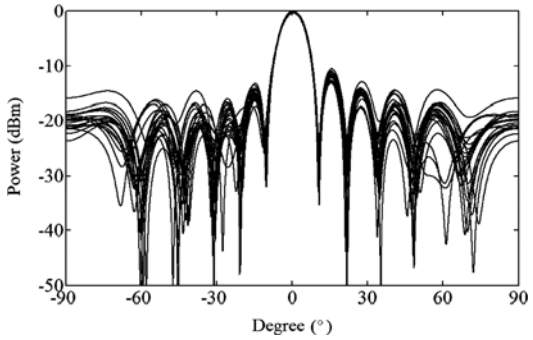

Fig. 6. Overlay of array patterns using 20 realizations of ILOA output phases, $N = 11$, $\sigma_f = 50$ MHz, and $Q = 10$.

TABLE III
COMPARISON OF ILOAs AND COAs

array type	ILOA	COA
mechanism	injection locking on each oscillator	mutual coupling between oscillators
governing equation	Adler's equation	generalized Adler's equation
control	all oscillators	two end oscillators (1)
coupling network	not required	required
external signal	required	not required
probability of lock	higher	lower
σ of beam-pointing error (at high Q)	larger	smaller
σ of beam-pointing error (at low Q)	smaller	larger
maximum inter-element phase difference	$180°/(N-1)$	$90°$

the array factor. Define the mean value of the beam-pointing error as

$$\langle\theta\rangle = \frac{1}{N_{\rm mc}} \sum_{s=1}^{N_{\rm mc}} \theta_s \tag{7}$$

where $N_{\rm mc}$ is the number of realizations in the Monte Carlo simulation, and θ_s is the zenith angle of the simulated major lobe in the sth realization. Similarly, the standard deviation of the beam-pointing error is defined as

$$\sigma_\theta = \sqrt{\frac{1}{N_{\rm mc}} \sum_{s=1}^{N_{\rm mc}} (\theta_s - \langle\theta\rangle)^2}. \tag{8}$$

Next, linear antenna arrays driven by ILOAs and COAs, respectively, are compared in terms of the beam-pointing error. The beam-pointing error is estimated on the locked cases. The quality factor of oscillators ranges from 10 to 20 in the X- and Ku-band [22]. Enhanced with a bond-wire inductor, the quality factor of oscillators on a CMOS substrate has been increased to over 50 in the X-band [25]. Hence, we choose $Q = 10$ and 62.832 in the simulations. From (4), the locking range is 500 MHz if $Q = 10$, and 79.577 MHz if $Q = 62.836$.

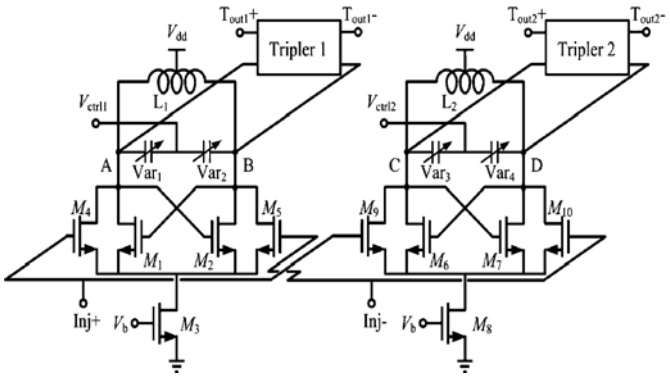

Fig. 7. Implementation of an ILOA with two VCOs and two frequency triplers.

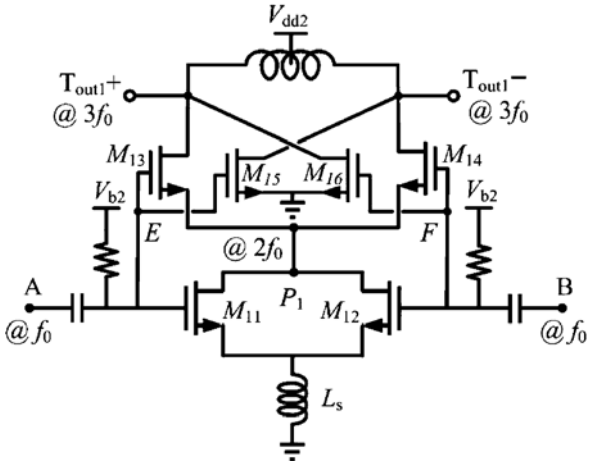

Fig. 8. Frequency tripler with high fundamental-rejection ratio.

Table I lists the simulated beam-pointing errors with the quality factor of each oscillator equal to 62.836. The standard deviation σ_f is chosen to be the same as in [26] for the convenience of comparison. Zhang *et al.* reported that the free-running frequency of a ring oscillator array at 1.3 GHz can be self-calibrated within a standard deviation, which is 2.79% of the center frequency [23]. Nogi *et al.* reported that oscillators with an average oscillation frequency of 12.45 GHz have a maximum deviation of 15 MHz [24].

The results of COAs match reasonably well with those in [26]. We then further adopt our numerical solver to analyze the case of the ILOA. It turns out that when $Q = 62.8$, the standard deviation, σ_θ, of COAs is lower than that of ILOAs. Table II lists the simulated beam-pointing errors with $Q = 10$. The standard deviation, σ_θ, of COAs is larger than that of ILOAs. These results imply that the synchronization of a COA demands high-Q oscillators to achieve better beam-pointing performance. If low-Q oscillators are used, using external injection signal leads to a better beam-pointing performance.

Fig. 5 shows the simulated standard deviation of the beam-pointing error, σ_θ, of the ILOA and COA, respectively, as a function of σ_f. It is observed that a larger ILOA exhibits lower σ_θ, while a smaller COA exhibits lower σ_θ.

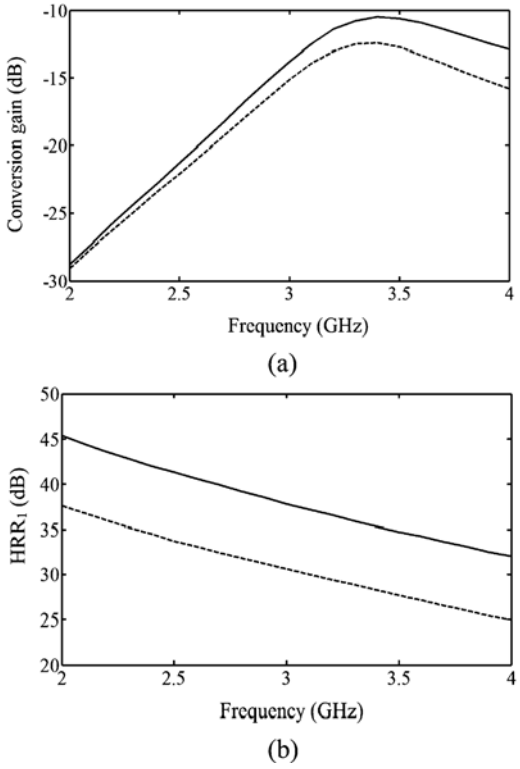

Fig. 9. Simulated: (a) conversion gain and (b) $1f$-isolation (HRR1) of the frequency tripler, —: with fundamental-canceling circuit, $-\ -\ -$: without fundamental-canceling circuit.

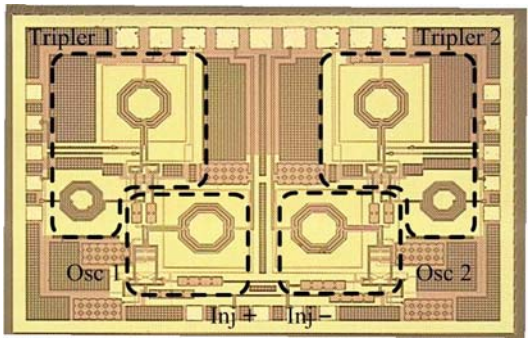

Fig. 10. Chip photograph of the ILOA fabricated in TSMC 0.18-μm CMOS technology.

The value of σ_θ listed in Table II looks small, but the effect of random frequency deviation on the overall pattern is obvious away from the major lobe. Fig. 6 shows the patterns derived from 20 realizations of output phases from the ILOA with $N = 11$, $\sigma_f = 50$ MHz, and $Q = 10$. The level variation is about 0.5 dB for the major lobe, and about 5 dB for the first sidelobe.

Table III summarizes the properties of ILOAs and COAs. One obvious disadvantage of an ILOA is that its maximum achievable inter-element phase difference is $180^\circ/(N-1)$, while that of a COA is $\pm 90^\circ$. ILOAs have been implemented using CMOS processes, which typically have a low Q value, techniques such as frequency doubling or tripling are required to increase the range of the beam-pointing angle.

IV. Implementation of an ILOA Chip

Fig. 7 shows an example of an ILOA, which consists of two modules, each module includes one oscillator and one frequency tripler. These two modules are fed with a common external signal. The ILOA is designed and implemented in 0.18-μm RF CMOS technology. The lossy substrate decreases the quality factor of the oscillators, making the ILOA a better choice in probability of lock and beam-steering error. The phase difference between these two oscillators can be controlled by tuning the free-running frequencies of both VCOs. To increase the available phase range, a frequency tripler is connected to the output of each oscillator.

Each VCO is a typical LC oscillator, with NMOS transistors M_1 and M_2 forming a cross-couple pair and M_3 serving as a current source. The differential external injection signal is fed to the gates of M_4 and M_5, which are in parallel with M_1 and

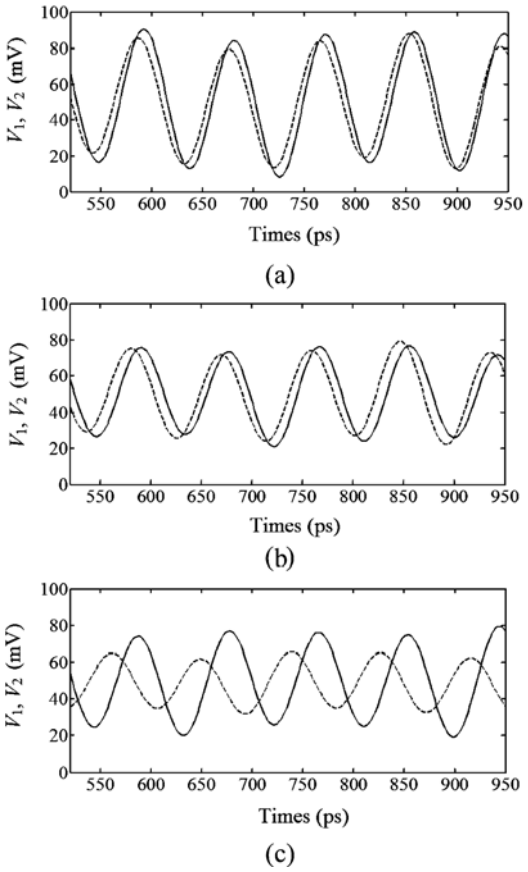

Fig. 11. Measured output waveforms of the ILOA. (a) $\alpha_z = 20^\circ$. (b) $\alpha_z = 40^\circ$. (c) $\alpha_z = 120^\circ$.

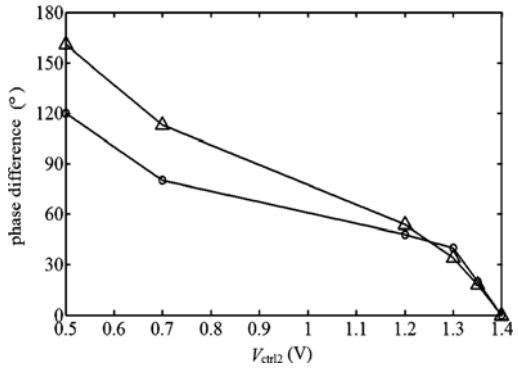

Fig. 12. Phase difference between two modules under different V_{ctrl2} when $V_{\mathrm{ctrl1}} = 1.4$ V, $-\triangle-$: simulation, $-\circ-$: measurement.

TABLE IV
COMPARISON OF OSCILLATOR ARRAYS

	this work	[5]	[11]	[29]	[30]
type	ILOA	ILOA	ILOA	COA with PLL	COA with PLL
injection frequency (GHz)	3.73	14.58-16.2	3.94	-	-
operation frequency (GHz)	11.2	43-48	3.94	7.4-9.4	2.67-2.72
phase range (°)	− 120 to 120	− 90 to 90	−47 to 47(3)	− 100 to 100	−16 to 52
phase resolution (°)	continuous	22.5(1)	continuous	continuous	continuous
element no.	2	4	2	4	3
total dc power (mW)	36	85(2)	460(4)	143(5)	-
technology	0.18 μm CMOS	65 nm CMOS	hybrid	45 nm CMOS SOI	hybrid

M_2, as shown in Fig. 7. The differential outputs at nodes A and B are directly connected to the frequency tripler.

Fig. 8 shows the schematic of the proposed frequency tripler, which is based on self-mixing of the fundamental (f_0) and the second-harmonic $(2f_0)$ signals. The second-harmonic signal is derived from a frequency doubler, which is composed of M_{11} and M_{12}. The input of the tripler is connected to the output of the oscillator. The signals at the gates of M_{11} and M_{12} are out of phase, and the drains of M_{11} and M_{12} are connected together. Hence, the second-harmonic common-mode signal appears at the common drain, which is the output of the doubler. Transistors M_{13} and M_{14} form a single-balanced up-conversion mixer, with their gates fed by the fundamental signal from the oscillator's output, and their sources connected to the output of the doubler. The doubler and the mixer shares the same dc current to reduce power consumption.

Frequency triplers based on self-mixing often suffer from low fundamental rejection ratio [27], [28]. In this design, a fundamental-canceling circuit, consisting of M_{15} and M_{16}, is adopted. Their gates are connected to the inputs of the frequency tripler, nodes E and F, and their drains are cross-connected to the output of the frequency tripler, as shown in Fig. 8. By properly tuning the sizes of (M_{13}, M_{14}) and (M_{15}, M_{16}), the fundamental signal can be canceled out at the output of the frequency tripler.

The fundamental-rejection ratio is defined as

$$\mathrm{HRR1} = P_{3f,\mathrm{out}} - P_{1f,\mathrm{out}} \tag{9}$$

where $P_{3f,\mathrm{out}}$ and $P_{1f,\mathrm{out}}$ are the output power (in dBm) of the desired signal at $3f_0$ and that of the fundamental signal at f_0, respectively. Fig. 9 shows the simulated conversion gain and HRR1 of the frequency tripler. The fundamental-canceling circuit increases the HRR1 by about 7.5 dB, and its conversion gain is increased by about 2.5 dB.

Fig. 10 shows a chip photograph of the proposed ILOA. The chip size is 1.42×0.97 mm^2, including the testing pads. The tuning range of the oscillator is from 3.5 to 3.95 GHz.

An Agilent E8257D signal generator is used to serve the input port of a coupler, with its isolated port terminated. The other two ports inject differential signals to the chip. No matching network is used between the chip and the coupler, and the differential signals are injected to the Inj+ and Inj− ports, as shown in Fig. 10 via a ground–signal–ground–signal–ground (GSGSG) probe. The injection frequency is 3.73 GHz, and the injection power to the input ports of the chip is around 5 dBm after calibration.

The frequency tuning range measured at tripler output is from 9.5 to 10.9 GHz. The measured phase noise is about −80 dBc/Hz at 1-MHz offset at the tripler output, estimated to be −89.5 dBc/Hz at the oscillator output using a phase noise cascade formula. The power consumption of the oscillator and the tripler is 10 and 8 mW, respectively.

The inter-element phase difference, α_z, between the two oscillators is tuned with the control voltages, V_{vctrl1} and V_{vctrl2}. Fig. 11 shows the output waveforms with $\alpha_z = 20°, 40°$ and 120°, respectively, measured by using an oscilloscope. The variation of envelope is attributed to the nonlinearity of the frequency tripler.

Fig. 12 shows the measured and simulated phase difference between two modules of the ILOA, where each module consisted of one oscillator and one frequency tripler. Oscillator 1 is treated as a phase reference with V_{ctrl1} fixed around 1.4 ± 0.1 V. The phase difference is measured between the outputs of the two triplers, and is adjusted by tuning V_{ctrl2}. When $V_{\mathrm{ctrl2}} = V_{\mathrm{ctrl1}}$, the free-running frequencies of both oscillators are the same and both oscillators are in phase. With $V_{\mathrm{ctrl2}} = 1.35$ V, the measured and simulated phase differences are 20° and 18°, respectively. With $V_{\mathrm{ctrl2}} = 1.3$ V, the measured and simulated phase differences are 40° and 34°, respectively.

The measured phase difference is 120° when $V_{\mathrm{ctrl1}} = 1.4$ V and $V_{\mathrm{ctrl2}} = 0.5$ V. By switching the control voltages to $V_{\mathrm{ctrl1}} = 0.5$ V and $V_{\mathrm{ctrl2}} = 1.4$ V, the phase difference becomes −120°. Hence, the available range of phase difference is from −120° to 120°. The lowest output power takes place when $V_{\mathrm{ctrl1}} = 1.4$ V and $V_{\mathrm{ctrl2}} = 0.5$ V, the simulated power level at tripler output port ($\mathrm{T}_{\mathrm{out1}+}$ in Fig. 7) is −13.6 dBm, and the measured output power is −16 dBm after calibration off the cable loss.

Table IV summarizes the properties of the proposed ILOA design in comparison with other oscillator arrays in the literature. The proposed design has a wider range of phase difference, attributed to the use of the frequency tripler. Note that PLLs are used in the designs of [29] and [30] to stabilize their COAs, and the COAs have lower probability of lock than ILOAs, based on the simulations in Section III.

V. Conclusion

The pros and cons of ILOAs and COAs have been reviewed based on Adler's equation. Both the probability of lock and beam-steering error are analyzed under different quality factors. The ILOAs have higher probability of lock than the COAs under both high Q and low Q conditions. The beam-pointing error of a uniform linear antenna array driven by the former is smaller than that driven by the latter under low Q condition. A two-element ILOA has been implemented in a low-Q CMOS process with a frequency tripler to increase the maximum range of inter-element phase difference. A fundamental-canceling circuit is also implemented to increase its harmonic suppression by 7.5 dB.

Acknowledgment

The authors would like to acknowledge fabrication and measurement support provided by the National Chip Implementation Center (CIC), Hsinchu, Taiwan.

References

[1] S. H. Yang and C. K. C. Tzuang, "130-nm CMOS K-band two-element differential power-combining oscillators," *IEEE Trans. Microw. Theory Techn.*, vol. 61, no. 3, pp. 1174–1185, Mar. 2013.

[2] J. Birkeland and T. Itoh, "A 16 element quasi-optical FET oscillator power combining array with external injection locking," *IEEE Trans. Microw. Theory Techn.*, vol. 40, no. 3, pp. 475–481, Mar. 1992.

[3] R. A. York and T. Itoh, "Injection and phase locking techniques for beam control," *IEEE Trans. Microw. Theory Techn.*, vol. 46, no. 11, pp. 1920–1929, Nov. 1998.

[4] P. Liao and R. A. York, "A new phase-shifterless beam-scanning technique using arrays of coupled oscillators," *IEEE Trans. Microw. Theory Techn.*, vol. 41, no. 10, pp. 1810–1815, Oct. 1993.

[5] L. Wu, A. Li, and H. C. Luong, "A 4-path 42.8-to-49.5 GHz LO generation with automatic phase tuning for 60 GHz phased-array receivers," *IEEE J. Solid-State Circuits*, vol. 48, no. 10, pp. 2309–2322, Oct. 2013.

[6] J. Lin and T. Itoh, "Active integrated antennas," *IEEE Trans. Microw. Theory Techn.*, vol. 42, no. 12, pp. 2186–2194, Dec. 1994.

[7] K. Chang, R. A. York, P. S. Hall, and T. Itoh, "Active integrated antennas," *IEEE Trans. Microw. Theory Techn.*, vol. 50, no. 3, pp. 937–944, Mar. 2002.

[8] R. A. York, "Nonlinear analysis of phase relationships in quasi-optical oscillator arrays," *IEEE Trans. Microw. Theory Techn.*, vol. 41, no. 10, pp. 1799–1809, Oct. 1993.

[9] K. D. Stephan and W. A. Morgan, "Analysis of inter-injection-locked oscillators for integrated phased arrays," *IEEE Trans. Antennas Propag.*, vol. AP-35, no. 7, pp. 771–781, Jul. 1987.

[10] R. Adler, "A study of locking phenomena in oscillators," in *Proc. IRE Waves Electrons.*, Jun. 1946, vol. 34, pp. 351–357.

[11] G. Forma and J. M. Laheurte, "Design for injection-locked oscillator arrays," *Electron. Lett.*, vol. 34, no. 7, pp. 683–684, Apr. 1998.

[12] T. D. Gathman and J. F. Buckwalter, "Injection locked oscillator arrays for spectrum analysis," in *IEEE RFIC Symp.*, 2009, pp. 575–578.

[13] V. Seetharam, J. Shen, and L. W. Pearson, "Effect of coupling phase on mutual injection locking range in coupled oscillator arrays," *IEEE Trans. Antennas Propag.*, vol. 57, no. 5, pp. 1391–1398, May 2009.

[14] W. A. Morgan and K. D. Stephan, "An X-band experimental model of a millimeter-wave interinjection-locked phased array system," *IEEE Trans. Antennas Propag.*, vol. 36, no. 11, pp. 1641–1645, Nov. 1988.

[15] Y.-T. Lo and J.-F. Kiang, "Analysis on strongly coupled oscillator arrays using modified Y-parameters approach," *Prog. Electromagn. Res. B*, vol. 59, pp. 71–87, 2014.

[16] B. Razavi, "A study of injection locking and pulling in oscillators," *IEEE J. Solid-State Circuits*, vol. 39, no. 9, pp. 1415–1424, Sep. 2004.

[17] W. H. Press, S. A. Teukolsky, W. T. Vetterling, and B. P. Flannery, *Numerical Recipes in C*, 2nd ed. Cambridge, U.K.: Cambridge Univ. Press, 1992, pp. 710–714.

[18] A. Mirzaei, M. E. Heidari, and A. A. Abidi, "Analysis of oscillators locked by large injection signals: Generalized Adler's equation and geometrical interpretation," in *IEEE Custom. Integ. Circuit. Conf.*, Sep. 2006, pp. 737–740.

[19] M. Thamsirianunt and T. A. Kwasniewski, "CMOS VCOs for PLL frequency synthesis in GHz digital mobile radio communications," *IEEE J. Solid-State Circuits*, vol. 32, no. 10, pp. 1511–1524, Oct. 1997.

[20] H. Akima, A. Dec, T. Merkin, and K. Suyama, "A 10 GHz frequency-drift temperature compensated *LC* VCO with fast-settling low-noise voltage regulator in 0.13 μm CMOS," in *IEEE Custom. Integ. Circuit. Conf.*, Sep. 2010, pp. 1–4.

[21] R. S. Elliott, *Antenna Theory and Design*, rev. ed. New York, NY, USA: Wiley, 2003, ch. 4.

[22] S. D. Toso, A. Bevilacqua, A. Gerosa, and A. Neviani, "A thorough analysis of the tank quality factor in *LC* oscillators with switched capacitor banks," in *Int. Circuit Syst. Symp.*, 2010, pp. 1903–1906.

[23] X. Zhang, I. Mukhopadhyay, R. Dokania, and A. B. Apsel, "A 46-μW self-calibrated gigahertz VCO for low-power radios," *IEEE Trans. Circuit Syst. II, Exp. Briefs*, vol. 58, no. 12, pp. 847–851, Dec. 2011.

[24] S. Nogi, J. Lin, and T. Itoh, "Mode analysis and stabilization of a spatial power combining array with strongly coupled oscillators," *IEEE Trans. Microw. Theory Techn.*, vol. 41, no. 10, pp. 1827–1837, Oct. 1993.

[25] K. Hu, F. Herzel, and J. C. Scheytt, "An X-band low-power and low-phase-noise VCO using bondwire inductor," *Adv. Radio Sci.*, vol. 7, pp. 243–247, 2009.

[26] J. Shen and L. W. Pearson, "The phase error and beam-pointing error in coupled oscillator beam-steering arrays," *IEEE Trans. Antennas Propag.*, vol. 53, no. 1, pp. 386–393, Jan. 2005.

[27] C. N. Kuo, H. S. Chen, and T. C. Yan, "A K-band CMOS quadrature frequency tripler using sub-harmonic mixer," *IEEE Microw. Wireless Compon. Lett.*, vol. 19, no. 12, pp. 822–824, Dec. 2009.

[28] Y. T. Lo and J. F. Kiang, "A 0.18 μm CMOS self-mixing frequency tripler," *IEEE Microw. Wireless Compon. Lett.*, vol. 22, no. 2, pp. 79–81, Feb. 2012.

[29] A. K. Gupta and J. F. Buckwalter, "A self-steering I/Q receiver array in 45-nm CMOS SOI," in *IEEE Radio Freq. Integ. Circuits Symp.*, Seattle, WA, USA, 2013, pp. 367–370.

[30] S. H. Yan and T. H. Chu, "A beam-steering antenna array using injection locked coupled oscillators with self-tuning of oscillator free-running frequencies," *IEEE Trans. Antennas Propag.*, vol. 56, no. 9, pp. 2920–2928, Sep. 2008.

Yu-Tsung Lo received the B.S., M.S., and Ph.D. degrees in electrical engineering from National Taiwan University, Taipei, Taiwan, in 2007, 2009, and 2014, respectively.

From 2010 to 2013, he worked part time with the National Chip Implementation Center (CIC), Hsinchu, Taiwan. Since July 2014, he has been with VIA Telecom (VTC), Taipei, Taiwan, as a Senior Engineer involved with CMOS cellular RF receiver design. During his graduate studies, he authored six journal papers on RFIC designs. His research interests include CMOS RF integrated circuits (RFICs), ultra-wideband (UWB) technology, and coupled oscillator arrays for beam-steering application.

Jean-Fu Kiang received the Ph.D. degree in electrical engineering from the Massachusetts Institute of Technology (MIT), Cambridge, MA, USA, in 1989.

Since 1999, he has been a Professor with the Department of Electrical Engineering and the Graduate Institute of Communication Engineering, National Taiwan University, Taipei, Taiwan. He has conducted research in electromagnetic applications, including antennas and arrays, wave propagation in ionosphere and atmosphere, satellite navigation, remote sensing, and microwave systems.